Research Article • DOI: 10.2478/amst-2019-0019 AMST • 44(3) • 2020 • 99-108

sciendo

Advances in Manufacturing Science and Technology

Control of kinetics of plasma assisted nitriding process of Ni-base alloys by substrate roughness

Wojciech J. Nowak*

Department of Materials Science, Faculty of Mechanical Engineering and Aeronautics, Rzeszów University of Technology, Powstanców Warszawy 12, 35-959 Rzeszów, Poland

Abstract

The present study investigated the effect of surface roughness on plasma assisted nitriding (PAN) process kinetics of Ni-base alloys. Two model alloys, namely Ni-10Cr and Ni-14Cr-4Al (wt.%) and commercial Rene 80, were examined. To elucidate the effect of surface roughness on nitriding kinetics, three methods of surface preparation were used, (1) polishing up with 1 μm diamond suspension, (2) grinding up to 220 grit sand-paper, and (3)grit blasting. The samples from each type of material were nitrided under the same conditions and investigated after processing. It was found that increase in roughness results in decreasing nitriding kinetics. The decrease of nitriding kinetics depends on alloy chemical composition, namely more complex chemistry resulted in smaller decrease of kinetics. Moreover, grit-blasting was found to be an improper method for surface preparation for PAN. The responsible mechanism for the effect of surface roughness on PAN kinetics of Ni-base alloys was proposed.

Keywords

plasma assisted nitriding, surface roughness, nitriding kinetics, Ni-base alloys

1. Introduction

The metallic elements used in automotive engines, jet engines, or gas turbines are often subject to adverse conditions due to abrasion or erosion resulting in failure of the component. So, the improvement of wear-resistance of such elements or their parts is necessary for a long life. Several techniques such as quenching, carburizing, boriding, nitriding, etc. are used for surface hardening. Nitriding is one of the most common methods used in which a hard layer is formed on surface of metals [1]. Nitriding is usually performed by several methods, such as liquid [2], gas [2, 3] or plasma nitriding [4]. The plasma nitriding can be carried out by either conventional direct current (DC) [5, 6] or pulsed DC [7–9]. Plasma assisted nitriding (PAN) is widely used for hardening of all kinds of steels, such as austenitic stainless steels [5], martensitic stainless steels [10, 11], precipitation hardening stainless steels [12], tool steels [13–14], or structural and constructional steels [15–17]. The hardening of steels is caused by high affinity of nitrogen to iron resulting in formation of phases like g'-Fe_4N, e-$Fe_{2-3}N$ or g_N (expanded austenite) [8]. Number of studies on nitriding of steels were performed. However, nitriding process of Ni-base alloys has created lot of interest to researchers. In this study, nitriding of Ni and Ni-base alloys were carried out on pure Ni and Ni-20Cr [18], Inconel 600 [19–21], Inconel 625 [22], Inconel 690 [23–25], and Inconel 718 [26, 27].

It was found that the key parameters influencing kinetics of plasma nitriding process are gas mixture [28, 29] and temperature [30, 31].

It was found that substrate roughness can strongly influence the oxidation behavior of Fe-base [32], Ni-base alloys, or even pure metals [33–36]. The change on the surface structure of metal was found when a surface preparation method, chemical vapor deposition (CVD) aluminizing, is carried out [37, 38]. It was claimed that surface roughness influences the kinetics of high temperature processes.

Despite the presence of many works about nitriding, no single work discusses the role of surface roughness of Ni-base substrates on nitriding plasma assisted kinetics when the process is carried out. Therefore, the aim of present work is to elucidate the effect of surface preparation method with different surface roughness on kinetics of plasma assisted nitriding of Ni-base alloys.

2. Materials and Methods

In the present study, two high purity (99.99%) Ni-base alloys and one commercially available Ni-based superalloy were investigated. The nominal chemical composition of studied alloys is given in

* *Corresponding author: Wojciech J. Nowak*
E-mail: w.nowak@prz.edu.pl

Table 1. Model alloys were manufactured by Goodfellow company in England in the form of rods with 10 mm diameter. Rene 80 was bought from Reade Advanced Materials in North America in the form of rod with 15 mm diameter. Coupons of 4 mm thick were machined from all materials. Each sample surface was prepared with different surface preparation method, namely polishing up to 1 mm, grinding till 220 grit SiC paper, and grit blasting. The representative samples, one per each surface preparation method, were subjected to treatment with respect to surface roughness description. Surface roughness was measured using laser profilometer Sensofar S-Neox Non-contact 3D Optical Profiler with vertical resolution 1 nm. After surface roughness evaluation, the samples were cleaned in ethanol, dried and treated by plasma assisted nitriding process (PAN). PAN was carried out using IONIT device at 590°C with the gas mixture consisting of N_2 with 25 dm^3/h flux and H_2 with 75 dm^3/h flux. The process was performed for 6 hours under 300 Pa using plasma with pulse 20/80 and frequency 10 kHz. After nitriding process, samples were subjected for post-processing characterization. Phase analyses were performed on selected nitrided samples using an X-ray diffractometer Miniflex II made by Rigaku. The 2q angle range varied between 20° and 120° and step size was 0.02°/s. Phase composition was determined using the Powder Diffraction File (PDF) developed and issued by the ICDD (The International Center for Diffraction Data). GD-OES depth profiling was performed using glow discharge optical emission spectrometer (GD-OES) made of Horiba Jobin Yvon. The GD-OES depth profiles were quantified using the procedure described in references [39–41]. After depth profiling, samples were coated with thin gold layer and subsequently electroplated with nickel and mounted in epoxy resin. Metallographic cross-sections of nitrided alloys' specimens were prepared using standard procedure. The cross-sections observations were done using light optical microscope (LOM) Nikon EPIPHOT 300 and analyzed by scanning electron microscope (SEM) Hitachi S3400N equipped with EDS and WDS detectors. Microhardness measurement was performed on the cross-sections using Micro-Combi Tester +CSM Instruments equipped with Berkovich indenter under 0.01 N load with acquisition rate 10 Hz and loading and unloading rate 0.02 N/min.

3. Results

3.1. Substrate roughness description

The surface roughness of representative materials prior to PAN process was evaluated by laser profilometer. Three-dimensional pictures of surfaces prepared by polishing, grinding, and grit blasting are shown in Figure 1A, B, and C, respectively. The differences in surface topography caused by different surface preparation method are clearly observed. However, the differences in *y*-axis should be highlighted. Laser profilometry is used to calculate roughness parameters, namely arithmetical mean height R_a and developed interfacial area ratio S_{dr}. Calculated values of roughness parameters are shown in Table 2. It is evidenced that different surface preparation method results in an increase of roughness parameters by at least one order of magnitude between polishing, grinding, and grit-blasting. However, a large increase in S_{dr} parameter representing surface to volume ratio, in case of grit-blasted surface should be mentioned.

3.2. Post-processing analyses

3.2.1. Model alloys

3.2.1.1. Ni-10Cr

GD-OES depth profiles obtained on polished, ground and grit-blasted Ni-10Cr model alloy after PAN process is shown in Figure 2A, B, and C, respectively. In case of polished and ground surfaces, a nitride zone is clearly visible as a region where nitrogen (N) content is increased in the early stage of depth profiling in comparison with later stages. As shown in Figure 2A, time for measuring increased N content is about 200 s, while for ground is up to 100 s. Such sharp zone of N enrichment is not observed in case of grit-blasted surface, rather uniform decrease of N profile is observed with increasing sputtering time. In both cases of clearly visible nitride zone, the measured N content is roughly about 10 at.%. The SEM/BSE images of the cross-sections of Ni-10Cr with differently prepared surfaces are depicted in Figure 3. As shown, looking from the top, the three characteristic zones can be observed: an electroplated Ni-coating, a nitrided layer, and a non-affected matrix material.

Table 1. The nominal chemical composition of studied alloys

Name of the alloy	Elements (wt.%)									
	Ni	Cr	Co	Mo	W	Al	Ti	Zr	B	C
Rene 80	BASE	14.00	9.50	4.00	4.00	3.00	5.00	0.03	0.02	0.16
Ni-14Cr-4Al	BASE	14.00	-	-	-	4.00	-	-	-	-
Ni-10Cr	BASE	10.00	-	-	-	-	-	-	-	-

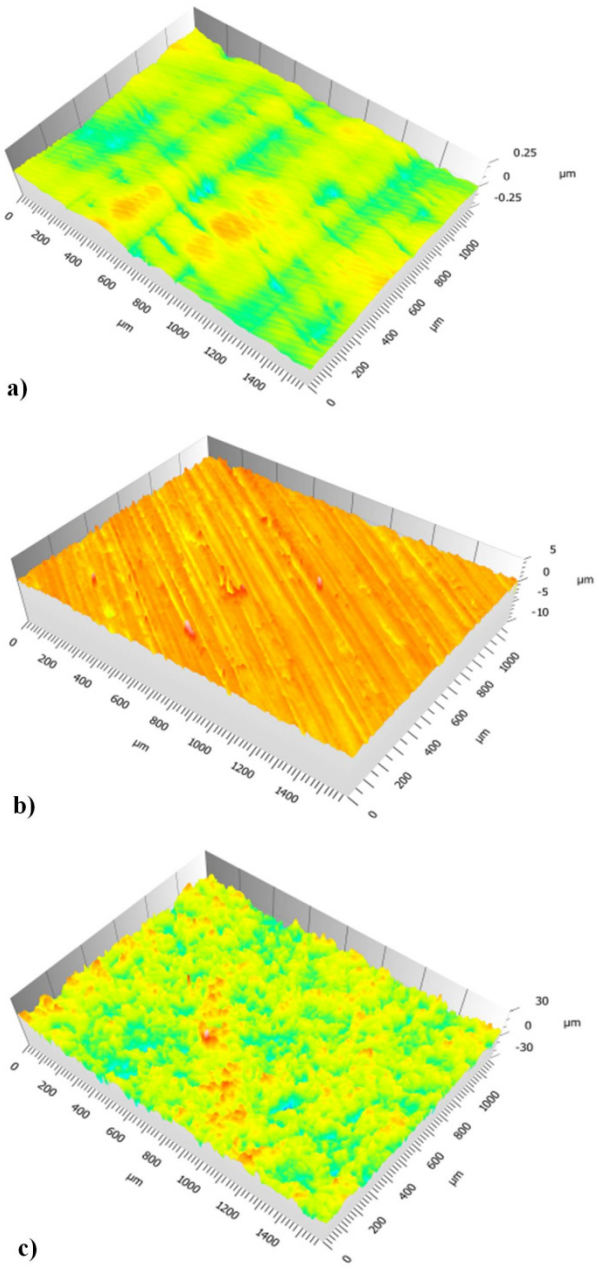

Figure 1. 3D reproduction of surface topography performed using laser profilometer on sample surfaces prepared by: (A) polished (1 mm), (B) ground (220 grit), and (C) grit blasting

Table 2. Calculated surface roughness parameters of alloy surfaces based on Figure 1

Roughness parameter	Surface preparation method		
	1 mm	220 grit	Grit-blasting
R_a (mm)	0.007890	0.235	3.16
S_{dr} (%)	0.000354	0.976	27.30

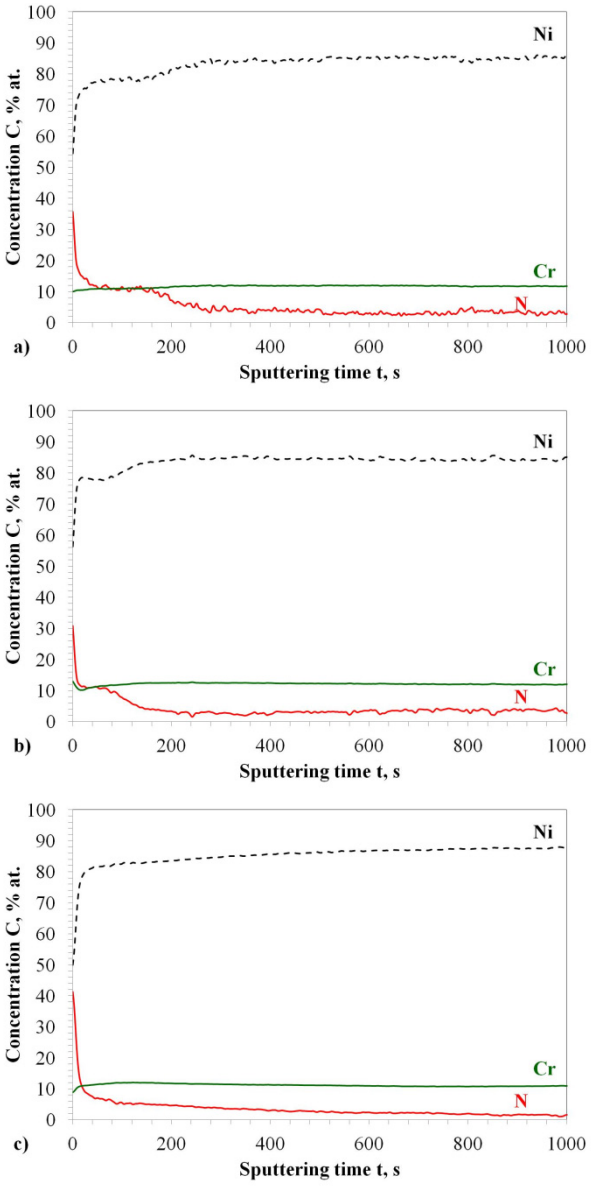

Figure 2. GD-OES depth profiles obtained on nitride Ni-10Cr model alloy with: (A) polished (1 mm), (B) ground (220 grit), and (C) grit-blasted surfaces

The latter is fully applicable for microstructure of polished and ground surfaces of Ni-10Cr alloy. Only local regions of nitrided material are observed for grit-blasted samples. Moreover, the embedded alumina particles are present in the near-surface region. One can clearly observe that thickness of nitrided layer is continuously higher for polished surface than that obtained for ground one. This observation is in agreement with GD-OES observation. Phase analysis performed by XRD revealed that the material after PAN process consists of two phases, namely matrix and Ni_3N.

3.2.2.2 Ni-14Cr-4Al

GD-OES depth profiles measured on Ni-14Cr-4Al nitrided alloy with different surface preparation method are shown in Figure 5. Similarly to observations on Ni-10Cr, a clear zone of nitrided layer of material is observed in Ni-14Cr-4Al with polished and ground surfaces. Moreover, as previously, longer time for measuring of nitrided layer is observed for polished material in comparison with ground one. However, it should be mentioned that the total time for measuring of nitrogen enrichment for polished Ni-14Cr-4Al is about 150 s and for ground one is about 75 s. Both sputtering times are shorter than those obtained for Ni-10Cr with polished and ground surfaces. Contrarily to observation for grit-blasted Ni-10Cr, a slight indication of nitrided layer is observed in grit-blasted Ni-14Cr-4Al, that is, nearly linear decreasing signal from nitrogen is observed up to 100 s of sputtering. SEM/BSE images (Figure 6) of the cross-sections of Ni-14Cr-4Al after nitriding process revealed a similar tendency as observed in Ni-10Cr, that is, thicker nitrided layer is observed for polished surface than for ground one. Moreover, in case of grit-blasted surface, a sign of nitrided layer is observed. Alumina particles in the near-surface region are observed as well. All these observations are similar to findings with GD-OES. Phase analysis revealed that nitriding results in formation of Ni_3N in Ni-14Cr-4Al matrix (see Figure 7).

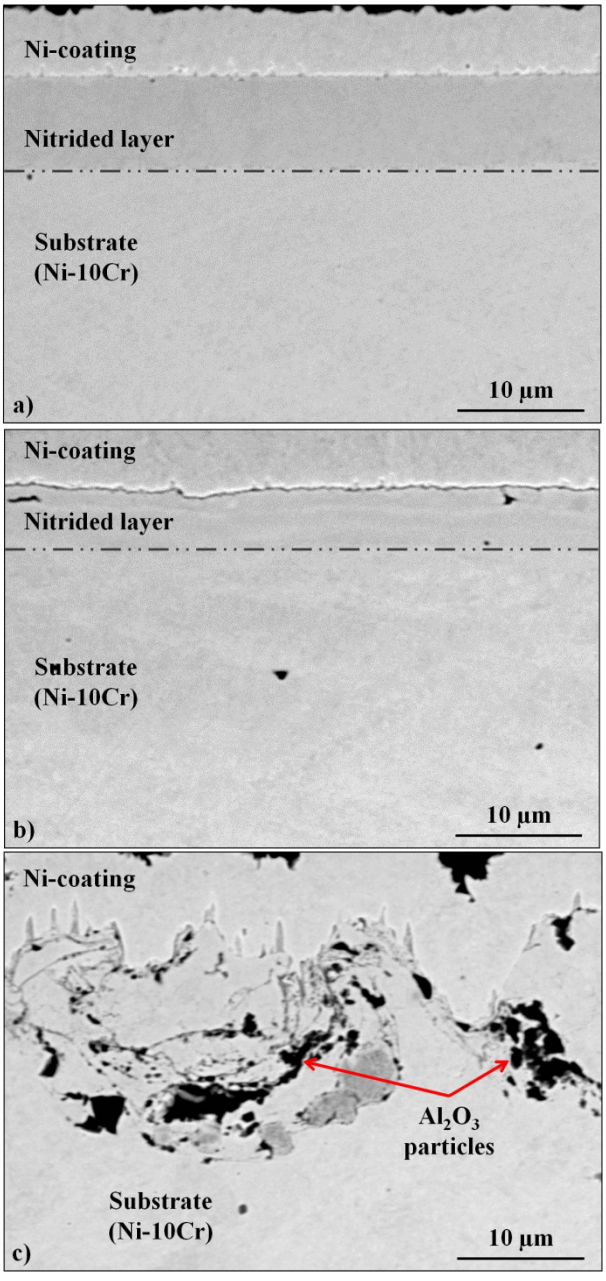

Figure 3. SEM/BSE images showing microstructure of nitrided Ni-10Cr model alloy with: (A) polished (1 mm), (B) ground (220 grit), and (C) grit-blasted surface

3.2.2. Commercial Ni-base alloy Rene 80

As shown in Figure 8, similar trends, as seen above, are observed in the commercial Ni-base superalloy Rene 80 in thickness of nitrided layer of polished, ground and grit-blasted surfaces. Nitrided layer formed on polished surface of the alloy (Figure 8A) is thicker than that on ground surface (Figure 8B). A zone of nitrided layer embedded with alumina particles is observed in grit-blasted Rene 80 (Figure 8C). Moreover, in all cross-sections, a g-g' microstructure is observed both in non-affected material core and nitrided zone (Figure 8).

4. Discussion

Nitriding process is usually used to produce a hard layer on surface of the elements exposed to abrasive atmosphere. Generally, hardening process by nitriding is carried out on Fe-based material. In the present study, PAN process is carried

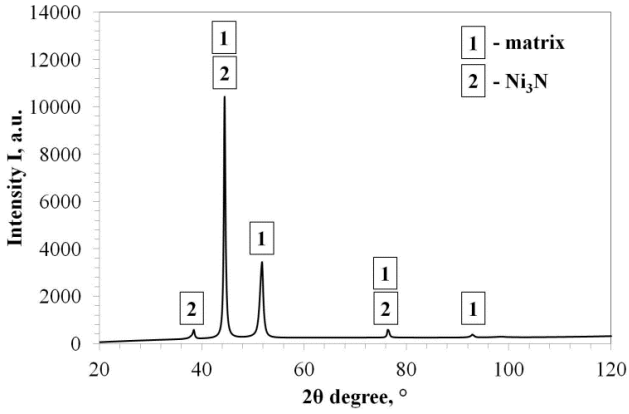

Figure 4. XRD patterns obtained from representative nitrided Ni-10Cr model alloy (polished (1 mm) surface).

out on Ni-base alloys. Therefore, microhardness tests were done on Ni-10Cr and Ni-14Cr-4Al alloys after PAN process. The locations of microhardness measurement points within the nitrided layers and matrix core on Ni-10Cr and Ni-14Cr-4Al are shown in Figure 9A and B, respectively. The increased numbers of indentation prints corresponding to measured hardness points are presented in Figure 9C at incremental distances from surface. The obtained results clearly indicated that PAN of Ni-base alloys results in hardening of material surface. When hardness of both materials are measured, a double increase in hardness is observed in the nitrided layer compared to core material. For Ni-10Cr the measured hardness in core material was about 100 HV whereas in nitrided layer it is about 250 HV. For Ni-14Cr-4Al, hardness measured in non-affected core material was 300 HV and in nitrided layer about 600 HV. The obtained results unequivocally show that Ni-base alloys are getting hardened by the formation of nitrided layer. Moreover, it is found that the hardness of bare Ni-10Cr is

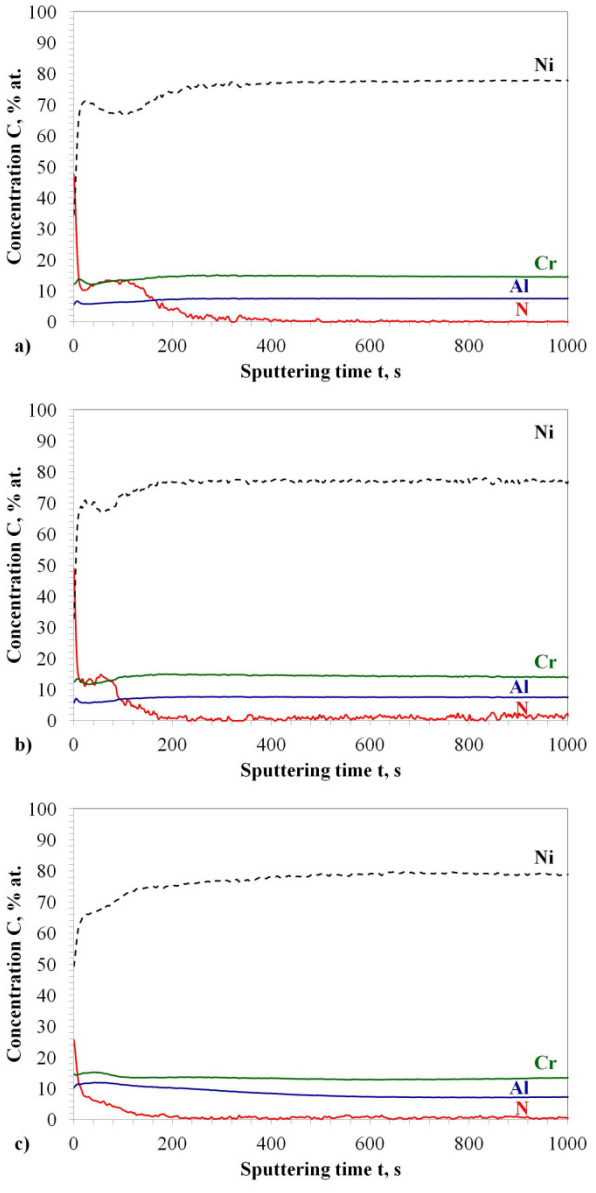

Figure 5. GD-OES depth profiles obtained on nitride Ni-14Cr-4Al model alloy with: (A) polished (1 mm), (B) ground (220 grit), and (C) grit-blasted surface

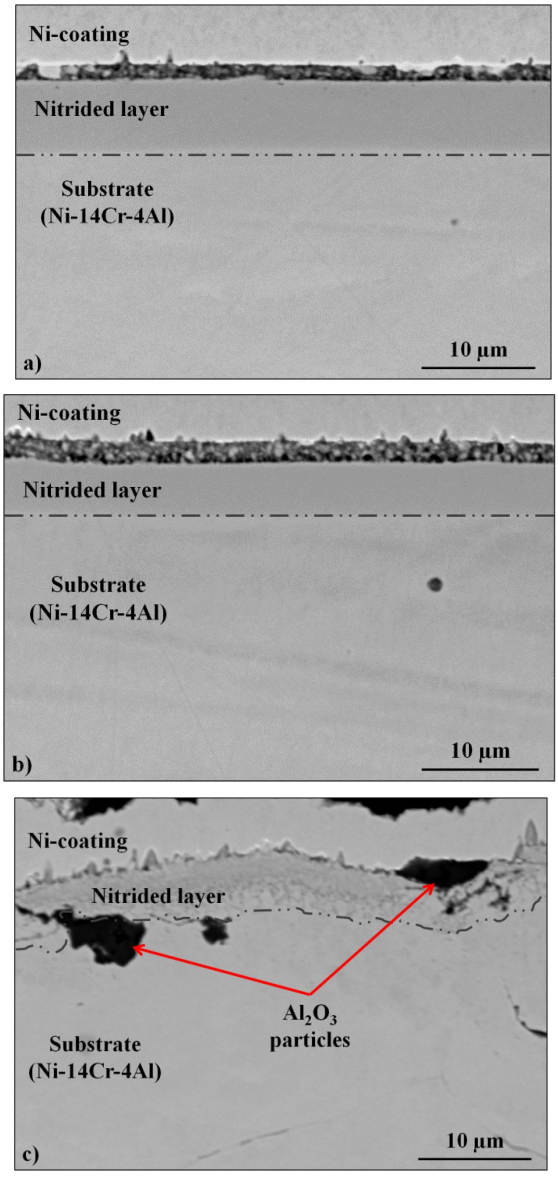

Figure 6. SEM/BSE images showing microstructure of nitrided Ni-14Cr-4Al model alloy with: (A) polished (1 mm), (B) ground (220 grit), and (C) grit-blasted surface

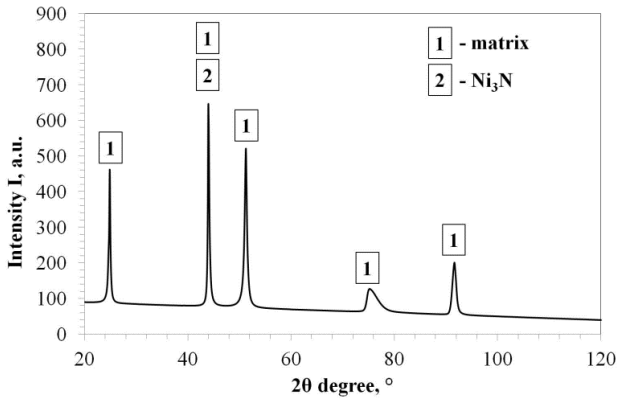

Figure 7. XRD patterns obtained from representative nitrided Ni-14Cr-4Al model alloy (polished (1 mm) surface).

three times smaller comparing to hardness of bare Ni-14Cr-4Al. The increase in hardness of alloy with complex chemical composition is caused by solid solution strengthening [42].

For elucidation the influence of surface roughness on kinetics of PAN of Ni-base alloys, cross-sections analysis was performed. Considering the fact that all materials were nitrided in the same conditions (i.e. using the same chamber, same temperature, and same time), simplified nitriding kinetics was done based only on nitrided layer thickness measurement. Three materials different in chemical composition were investigated, however, in one material, the surface roughness has become an important variable. Then, the influence of surface preparation method resulting in different surface roughness was directly investigated. The surface prepared by polishing (smooth surface) results in higher thickness of nitrided layer. Grinding causes decrease in the nitrided layer thickness of all materials. However, one should highlight, that the highest effect of surface roughness is observed in the simplest material, namely Ni-10Cr, for which the biggest decrease in average thickness of nitrided layer is observed, that is the nitride layer thickness 7 mm for a polished material is reduced to 4 mm for a grinding material, a drop of 40%. Similarly 35% drop is observed for Ni-14Cr-4Al which means that the average thickness is reduced by 2 mm, from 6 mm to 4 mm. But in commercially available Ni-base superalloy Rene 80, only a slight variation (10% drop) in nitrided layer thickness was observed between polished (4.2 mm) and ground (3.8 mm) surfaces. Nevertheless, the trend is similar to that observed on model alloys. Then, one can conclude, that nitriding kinetics depends on surface roughness, however, more complex chemistry of studied alloy hinders this effect. In grit-blast materials, average thickness of nitrided layer is higher than that of ground one, but the thickness is not uniform and varied according to the material composition. So we can say mathematically that standard deviation of the measurement is relatively high. Analysis of cross-sections by optical microscope (Figure 10) also confirmed the findings for the grit-blast material. The images of the optical microscope taken at low magnification show the formation of nonuniform layer in all studied materials (Figure 10). Moreover, numerous alumina particles embedded in the near-surface region of the alloys are found. In many cases, no nitrided layer is found in the neighborhood of alumina particles. So all the above mentioned observations prove that grit-blast method surface

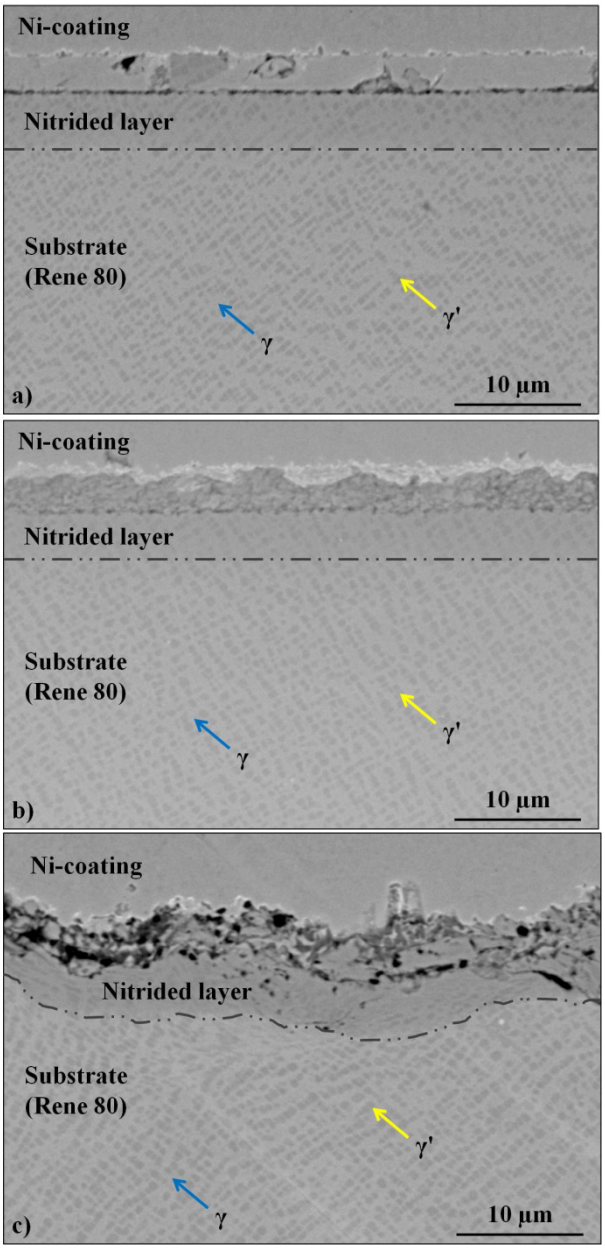

Figure 8. SEM/BSE images showing microstructure of nitrided Rene 80 with: (A) polished (1 mm), (B) ground (220 grit), and (C) grit-blasted surface

preparation method is not a suitable one for nitriding process. Based on the results obtained from the present work, a following mechanism responsible for the effect of surface roughness on kinetics of PAN is proposed as follows. Figure 11A represents the situation prior to gas ionization (i.e. prior to plasma burn). As shown, between positively charged anode and negatively charged cathode, a mixture of N_2 and H_2 is present. As the samples are electrically conductive and act as cathodes the surfaces of the samples are negatively charged. After plasma burning, gas becomes ionized, and positively charged N^+ ions and electrons are produced (Figure 11B). Then, due to differences in charge, positively charged nitrogen ions become attracted and accelerated toward negatively charged samples' surfaces. In the process surface gets heated, the nitrogen ions are built up into the near-surface region of the samples. However, as shown in Figure

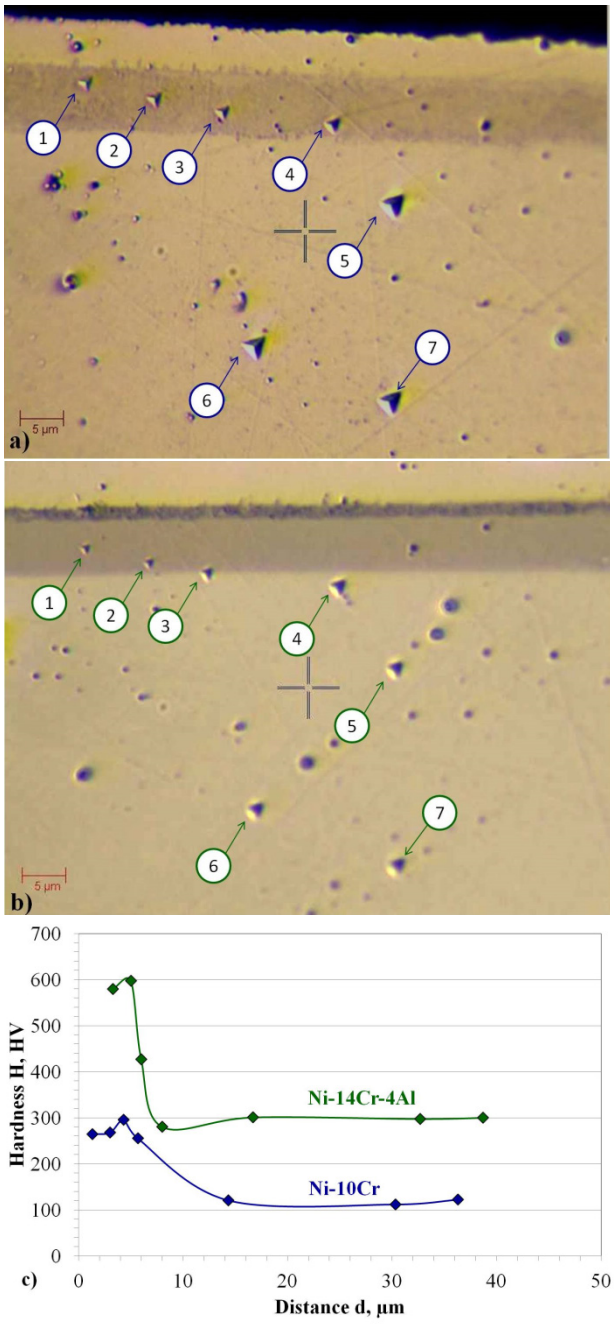

Figure 9. Images showing indentation prints after hardness measurement obtained on: (A) Ni-10Cr (polished (1 mm)), (B) Ni-14Cr-4Al (polished (1 mm)), and (C) a plot with hardness profile obtained as function of distance from surface

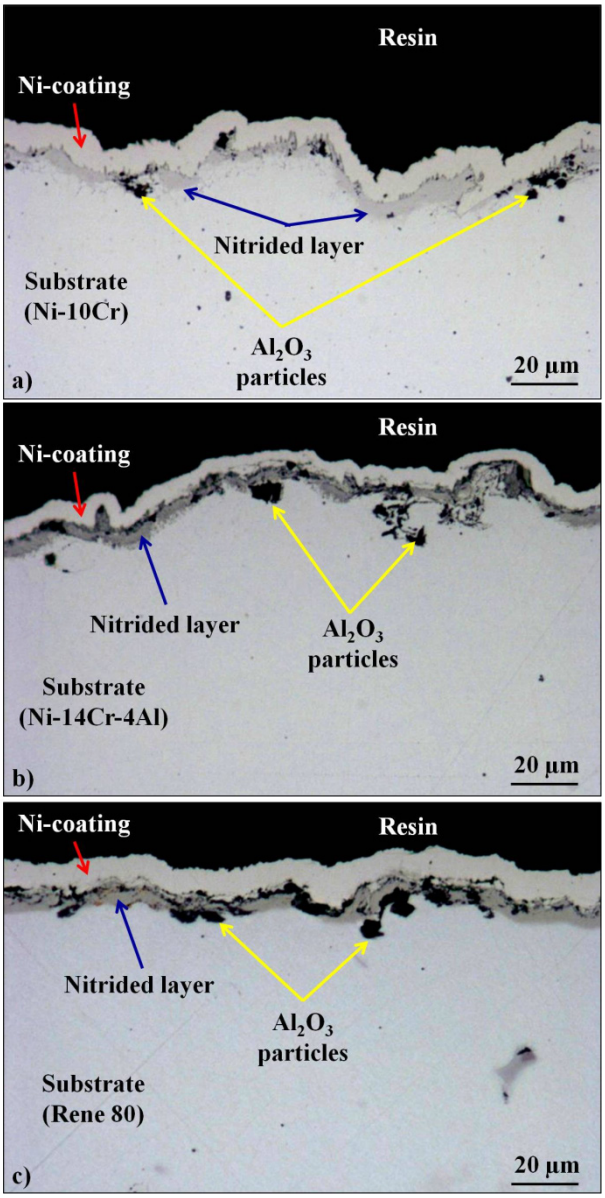

Figure 10. Images showing microstructure of nitride layer formed on grit-blasted surfaces of: (A) Ni-10Cr, (B) Ni-14Cr-4Al and (C) Rene 80 captured by optical microscope

11B, in case of polished surface, the charge distribution is uniform over whole surface, while in case of ground surface a presence of hills and valleys (not uniform) are observed. Since charge tends to accumulate at convex regions of a conductor [43] then, in the latter case, positively charged nitrogen ions are preferentially attracted by the hills and implanted in those regions. Implantation of N-ions results in local expansion of the lattice. As implantation of ions gets saturated, their further entry is controlled by diffusion flux in solid state (Figure 11C). In case of ground surface, nitrogen is preferentially implanted to top of the hills resulting in a bottle neck in nitrogen transport. This in turn results in the movement of smaller number of nitrogen into the near-surface region when compared with polished one. The diffusion flux depends on the number of adsorbed atoms, then higher number of implanted atoms results in higher diffusion flux and the same in higher PAN kinetics. Therefore, in the present work, it is proposed that preferential implantation of nitrogen ions in the hills is responsible for formation of thinner nitrided layer on top of rougher surface.

5. Conclusions

The results obtained in the frame of present work allow to formulating the following conclusions:

Plasma assisted nitriding of Ni-base alloy results in formation of hard nitrided coating. The increase in coating hardness depends on alloy chemical composition, however, at least double increase in HV between bare material and nitrided coating was found in present study.

Surface preparation method resulting in different surface roughness actively influences the kinetics of plasma assisted nitriding process. Increasing surface roughness adversely influences the nitriding kinetics. Surface smoothening increases kinetics of plasma assistednitriding . Then, shortening of plasma assisted nitriding by surface preparation is proposed.

More complex chemical composition of the alloy hinders the effect of surface roughness on PAN kinetics.

Grit-blasting causes formation of nonuniform and not continuous nitrided layer which disqualifies surface preparation of materials using blasting parameters is shown in the present work for PAN.

Mechanism responsible for the effect of surface roughness on PAN kinetics is proposed.

Acknowledgments

The author gratefully acknowledges Marek Poręba, PhD Eng., and Wojciech Cmela, MSc., for performing plasma

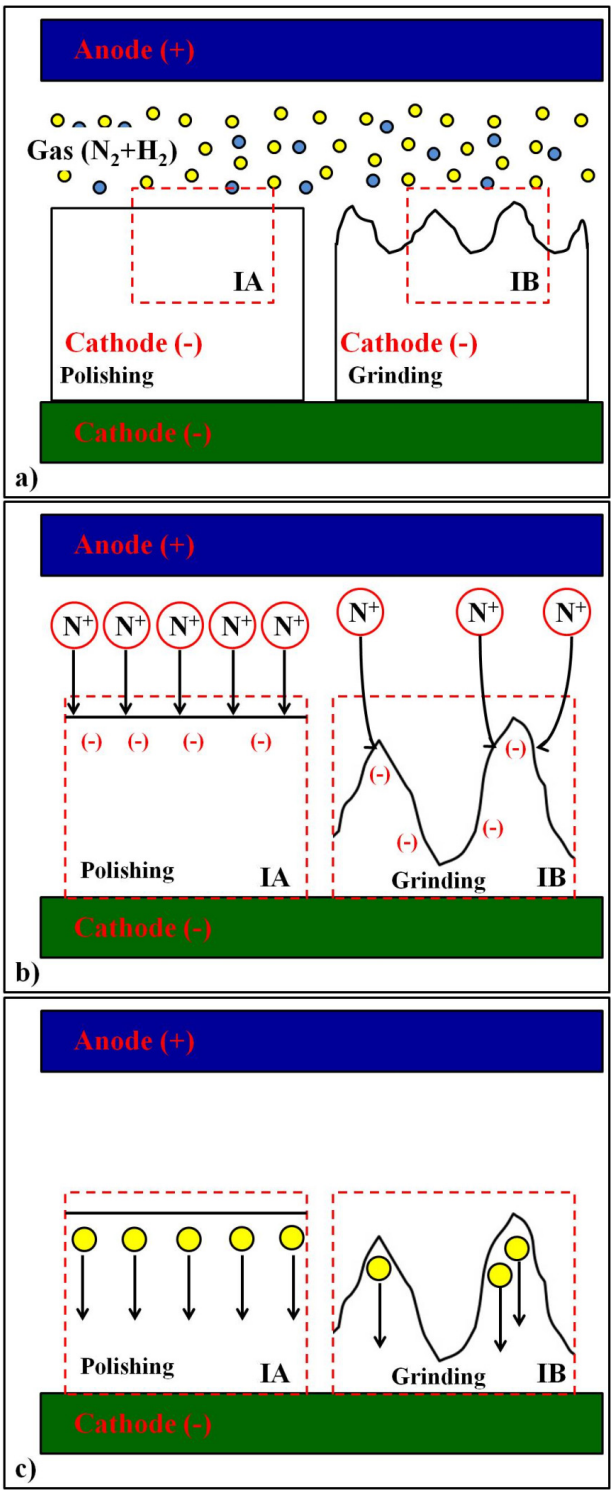

Figure 11. Proposed mechanism responsible for effect of surface roughness profile on effective nitride layer depth showing: (A) prior to gas ionization, (B) situation with ionized gas, and (C) with implanted nitrogen into near-surface region.

assisted nitriding process and Krzysztof Krupa, PhD, for microhardness analysis. Elżbieta Michno, MSc Eng., is also gratefully acknowledged for the preparation of samples.

Funding

Project financed by the National Center for Research and Development (Narodowe Centrum Badań i Rozwoju) under the TECHMATSTRATEG2/406725/1/NCBR/2020 program.

References

[1] F. CZERWINSKI: Heat treatment-conventional and novel applications. InTech, Rijeka, 2012.

[2] H. CHANDLER: Heat Treater's Guide: Practices and Procedures for Irons and Steels, ASM International, Ohio 1995.

[3] J.R. DAVIS: Surface hardening of steels. ASM International, Ohio 2002.

[4] R. CHATTOPADHYAY: Advanced thermally assisted surface engineering processes. Kluwer Academic Publisher, Dordrecht 2004.

[5] M. EGAWA, et al.: Effect of additive alloying element on plasma nitriding and carburizing behavior for austenitic stainless steels. *Surf. Coat. Technol*., **205**(2010), 246-251, DOI: 10.1016/j.surfcoat.2010.07.093.

[6] J.X. WANG, et al.: Effects of DC plasma nitriding parameters on microstructure and properties of 304L stainless steel. *Mater. Charact*., **60**(2009), 197-203, DOI:10.1016/j.matchar.2008.08.011.

[7] M. NAEEM, et al.: Influence of pulsed power supply parameters on active screen plasma nitriding, *Surf. Coat. Technol*., **300**(2016), 67-77, DOI:10.1016/j.surfcoat.2016.05.032.

[8] H. AGHAJANI, S. BEHRANGI: Pulsed DC glow discharge plasma nitriding. In: Plasma Nitriding of Steels, Topics in Mining, Metallurgy and Materials Engineering. Springer, Cham 2017.

[9] S. YANG, et al.: Effect of nitriding time on the structural evolution and properties of austenitic stainless steel nitrided using high power pulsed DC glow discharge Ar/N2 plasma. *J. Coat. Sci. Technol*., **3**(2016), 62-74, DOI:10.6000/2369-3355.2016.03.02.3.

[10] I. ALPHONSA, et al.: A study of martensitic stainless steel AISI 420 modified using plasma nitriding. *Surf. Coat. Technol*., **150**(2002), 263-268, DOI:10.1016/S0257-8972(01)01536-5.

[11] K. WU, et al.: Research on new rapid and deep plasma nitriding techniques of AISI 420 martensitic stainless steel. *Vac*., **84**(2010), 870-875, DOI: 10.1016/j.vacuum.2009.12.001.

[12] J.R. SOBIECKI, P. MAŃKOWSKI, A. PATEJUK: Improving the performance properties of valve martensitic steel by glow discharge-assisted nitriding. *Vac*., **76**(2004), 57-61, DOI:10.1016/j.vacuum.2004.05.020.

[13] Y. BIROL: Response to thermal cycling of plasma nitrided hot work tool steel at elevated temperatures: *Surf. Coat. Technol.,* **205**(2010), 597-602, DOI: 10.1016/j.surfcoat.2010.07.035.

[14] A. DA SILVA ROCHA, et al.: Microstructure and residual stresses of a plasma-nitrided M2 tool steel. *Surf. Coat. Technol*., **115**(1999), 24-31, DOI: 10.1016/S0257-8972(99)00063-8.

[15] S. KARAOGLU: Structural characterization and wear behavior of plasma-nitrided AISI 5140 low-alloy steel. *Mater. Charact*., **49**(2003), 349-357, DOI:10.1016/S1044-5803(03)00031-7.

[16] M. KARAKAN, A. ALSARAN, A. ÇELIK: Effects of various gas mixtures on plasma nitriding behavior of AISI 5140 steel. *Mater. Charact*., **49**(2003), 241-246, DOI:10.1016/S1044-5803(03)00010-X.

[17] F. MAHBOUBI, K. ABDOLVAHABI: The effect of temperature on plasma nitriding behavior of DIN 1.6959 low alloy steel. *Vac*., **81**(2006), 239-243, DOI:10.1016/j.vacuum.2006.03.010.

[18] F. PEDRAZA, et al.: Low-energy high-flux nitriding of Ni and Ni20Cr substrates. *Surf. Coat. Technol*., **176**(2004), 236-242, DOI:10.1016/S0257-8972(03)00735-7.

[19] F. MINDIVANA, AND H. MINDIVAN: Comparisons of wear performance of hardened Inconel 600 by different nitriding processes. *Procedia Eng*., **68**(2013), 730-735, DOI:10.1016/j.proeng.2013.12.246.

[20] Y. SUN: Kinetics of layer growth during plasma nitriding of nickel based alloy Inconel 600. *J. Alloys Compd*., **351**(2003), 241-247, DOI:10.1016/S0925-8388(02)01034-4.

[21] C. SUDHA, et al.: Nitriding kinetics of Inconel 600. *Surf. Coat. Technol*., **226**(2013), 92-99, DOI: 10.1016/j.surfcoat.2013.03.040.

[22] T. BOROWSKI, et al.: Modifying the properties of the Inconel 625 nickel alloy by glow discharge assisted nitriding. *Vac*., **83**(2009), 1489-1493, DOI: 10.1016/j.vacuum.2009.06.056.

[23] H. HE, et al.: Stress induced anisotropic diffusion during plasma-assisted nitriding of a ni-based alloy. *Mater. Sci. Forum,* **475-479**(2005), 3669-3672, DOI: 10.4028/www.scientific.net/MSF.475-479.3669.

[24] C. LEROY, et al.: Plasma assisted nitriding of Inconel 690. *Surf. Coat. Technol*., **142–144**(2001), 241-247, DOI:10.1016/S0257-8972(01)01243-9.

[25] Y.C. SHARMA, et al.: Low temperature plasma ion nitriding (PIN) of Inconel 690 alloy. *Mater. Res. Express*, **6**(2018), 026559. DOI:10.1088/2053-1591/aaf1f3.

[26] H. KOVACÍ, et al.: Effect of plasma nitriding parameters on the wear resistance of alloy Inconel 718. *Met. Sci. Heat Treat*., **58**(2016), 470-474, DOI: 10.1007/s11041-016-0037-1.

[27] K. VENKATESAN, R. RAMANUJAM, P. KUPPAN: Parametric modeling and optimization of laser scanning parameters during laser assisted machining of Inconel 718. *Opt. Laser Technol*., **78**(2016), 10-18, DOI: 10.1016/j.optlastec.2015.09.021.

[28] N.Z. NEGM: A study on RF plasma nitriding at a constant power in different H_2–N_2 mixtures at different temperatures. *Mater. Sci. Eng. B*, **129**(2006), 207-210, DOI: 10.1016/j.mseb.2006.01.015.

[29] F.Z. BOUANIS, et al.: Study of corrosion resistance properties of nitrided carbon steel using radiofrequency N_2/H_2 cold plasma process. *Corros. Sci*. **52**(2010), 3180-3190, DOI: 10.1016/j.corsci.2010.05.021.

[30] K.H. PRABHUDEV: Handbook of heat treatment of steels. McGraw-Hill, New Delhi 2005.

[31] G.E. TOTTEN: Steel heat treatment hand book, Equipment and Process Design, Taylor & Francis Group, Boca Raton 2007.

[32] W.J. NOWAK, D. SERAFIN, B. WIERZBA: Effect of surface mechanical treatment on the oxidation behavior of FeAl-model alloy, *J. Mater. Sci*., **54**(2019), 9185-9196, DOI:10.1007/s10853-019-03509-5.

[33] W.J. NOWAK: Effect of surface roughness on early stage oxidation behavior of Ni-Base superalloy IN 625. *Appl. Sys. Innov*., **1**(2018)3, 32, DOI: 10.3390/asi1030032.

[34] W. J. NOWAK, B. WIERZBA: Effect of surface treatment on high temperature oxidation behavior of IN 713C. *J. Mater. Eng. Perform*. **27**(2018)10, 5280-5290, DOI:10.1007/s11665-018-3621-2.

[35] D. SERAFIN, W.J. NOWAK, B. WIERZBA: The effect of surface preparation on high temperature oxidation of Ni, Cu and Ni-Cu alloy. *Appl. Surf. Sci*. **476**(2019), 442-451, DOI:10.1016/j.apsusc.2019.01.122.

[36] D. SERAFIN, W.J. NOWAK, B. WIERZBA: Mechanically prepared copper surface in oxidizing and non-oxidizing conditions. *Appl. Surf. Sci*., **492**(2019), 607-616, DOI:10.1016/j.apsusc.2019.06.231.

[37] W.J. NOWAK, et al.: Effect of substrate roughness on oxidation resistance of an aluminized Ni-Base superalloy. *Metals*, **9**(2019), 782-795, DOI:10.3390/met9070782.

[38] W.J. NOWAK, et al.: Durability of underaluminized thermal barrier coatings during exposure at high temperature. *Surf. Coat. Technol*. **382**(2020), 125236, DOI:10.1016/j.surfcoat.2019.125236.

[39] J.P. PFEIFER, et al.: Quantitative analysis of oxide films on ODS-alloys using MCs+-SIMS and e-beam SNMS. *J. Anal. Chem*., **346**(1993), 186-191, DOI:10.1007/BF00321410.

[40] W.J. QUADAKKERS, et al.: Composition and growth mechanisms of alumina scales on FeCrAl-based alloys determined by SNMS. *Appl. Surf. Sci*. **52**(1991), 271-287, DOI:10.1016/0169-4332(91)90069-V.

[41] W.J. NOWAK: Characterization of oxidized Ni-based superalloys by GD-OES. *J. Anal. At. Spectrom*., **32**(2017), 1730-1738. DOI:10.1039/C7JA00069C.

[42] J.T. BLACK, R.A. KOHSER: DeGarmo's materials and processes in manufacturing, Eleventh Edition. Wiley, Hoboken 2012.

[43] R. CADE, D. OWEN: Charge density, vertices and high curvature in two-dimensional electrostatics. *J. Electrostat*., **17**(1985), 125-136, DOI:10.1016/0304-3886(85)90015-4.